Received 21 October 2024; revised 22 November 2024; accepted 5 December 2024. Date of publication 11 December 2024; date of current version 23 December 2024. The review of this article was arranged by Associate Editor Lei Gu.

Digital Object Identifier 10.1109/OJPEL.2024.3515798

Extending the Steinmetz Equation: Incorporating Mechanical Stress Effects in Ferrite Core Loss Calculations

JANNIK SCHÄFER (Member, IEEE), GWENDOLIN ROHNER, AND JOHANN W. KOLAR (Life Fellow, IEEE)

Power Electronic Systems Laboratory, ETH Zurich, 8092 Zurich, Switzerland

CORRESPONDING AUTHOR: JANNIK SCHÄFER (e-mail: schaefer@lem.ee.ethz.ch)

This article has supplementary downloadable material available at https://doi.org/10.1109/OJPEL.2024.3515798, provided by the authors.

ABSTRACT This paper extends the Generalized Steinmetz Equation (GSE) to account for the influence of mechanical stress on ferrite core losses. Experimental measurements are used to quantify the effects of compressive and tensile stresses on the relative permeability and the core losses of different ferrite materials. Mechanical stress is found to significantly affect the core losses, depending on the relative orientation of the magnetic flux density and the applied mechanical stress. Specifically, the losses monotonically increase when the flux and compressive stress vectors are parallel, while perpendicular vectors lead to a more complex response depending on the level of mechanical stress. The measured loss characteristics are translated in an extension of the GSE (X-GSE), which is validated for different ferrite materials, and provides a useful tool for a first rough estimation of the core losses under mechanical stresses. Finally, FEM simulations demonstrate how thermally induced mechanical stresses in a ferrite core can redistribute the magnetic flux and therefore impact the resulting core losses, which underlines the importance of considering the stress dependence of core losses in ferrite, especially in the development of magnetic components to be encapsulated in incompressible materials.

INDEX TERMS Core loss modeling, ferrite core losses, magnetic materials, mechanical stress, Steinmetz equation.

I. INTRODUCTION

Accurate modeling of core losses is a crucial aspect of designing magnetic components, as it enables the development of compact, cost-effective, and reliable inductors and transformers. If relevant loss mechanisms are not properly considered, the designed magnetic components can easily overheat in the final application. This overheating can lead to a thermal runaway, driven by the temperature dependence of core losses, potentially resulting in irreversible damage to the components.

However, accurately predicting core losses in ferrite is challenging due to their dependence on numerous physical quantities, often in highly nonlinear ways, as visually illustrated in Fig. 1 (without quantitative significance). Early efforts to model core losses in ferrites aimed to capture the dependence of the core losses on the operating frequency f_B and amplitude $\hat{B}$ of a sinusoidal magnetic excitation as simply as possible [1]. This led to the development of the Generalized Steinmetz Equation (GSE) [2]

$$p_C = C \cdot f_B^{\alpha} \cdot \hat{B}^{\beta}, \quad (1)$$

which provides reasonable accuracy for sinusoidal magnetic excitations. With the advent of switch-mode power supplies, the GSE was extended to be applicable to non-sinusoidal excitations, resulting in the modified Steinmetz equation (MSE) [3] and in a next step in the improved GSE (iGSE) [4]. Subsequently, the impact of a DC bias in the magnetic excitation on the core losses has been investigated, resulting in DC bias-dependent Steinmetz parameters [5]. Next, the temperature dependence was incorporated through an additional Steinmetz parameter [6], and the iGSE was expanded with five additional parameters, accounting for various additional core loss mechanisms such as relaxation effects in non-sinusoidal excitations, culminating in the i^{2}GSE [7].

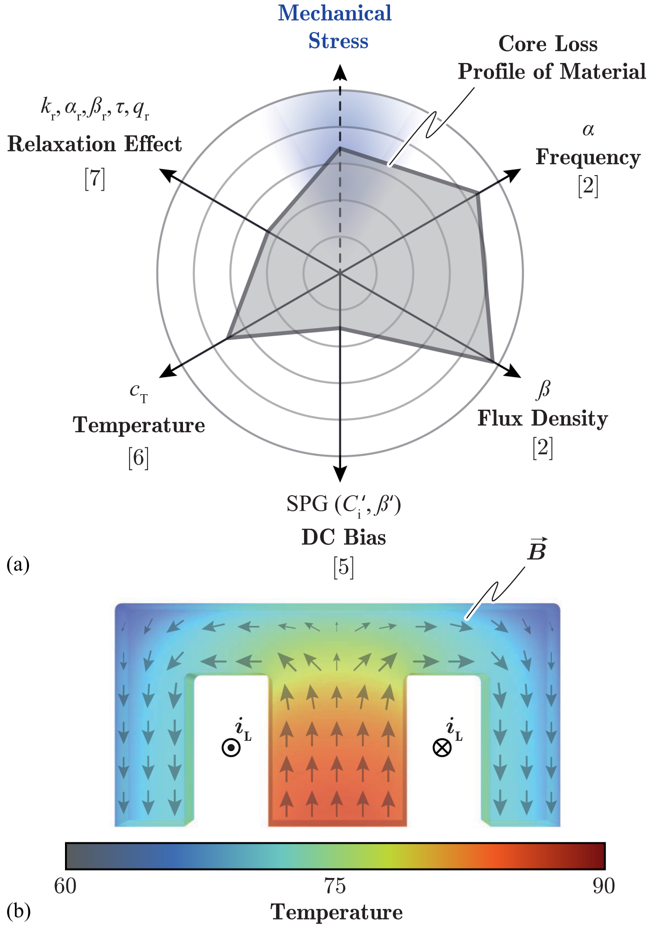

FIGURE 1. **(a) Visual representation of the dependencies of core losses in a ferrite material on various operating parameters including the corresponding Steinmetz parameters (α, β, C_i', β', c_T, k_r, α_r, β_r, τ, q_r), where SPG stands for "Steinmetz Premagnetization Graph". (b) Exemplary temperature and flux density distribution in an E-core of a conventional inductor arrangement assuming forced convection.**

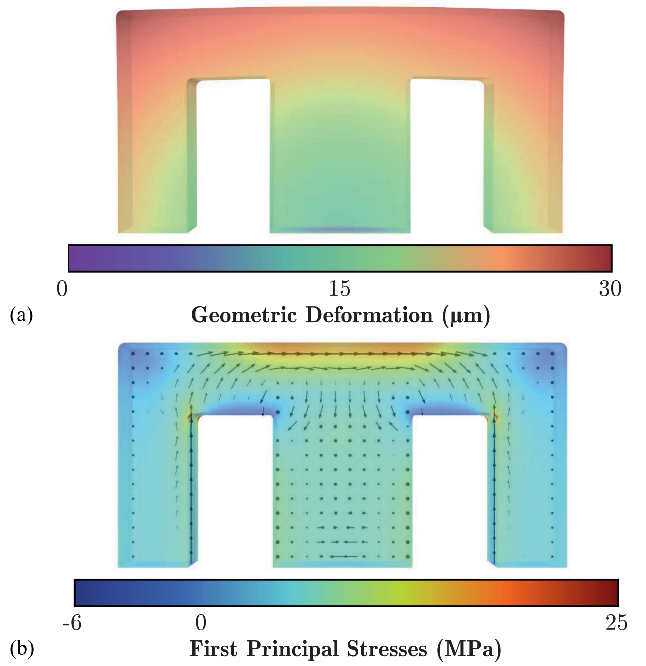

FIGURE 2. **(a) Simulated geometric displacement of the E-core of Fig. 1(b) due to the thermal expansion of the material and (b) first principal stresses in the core, which occur due to the inhomogeneous thermal expansion of the material and its stiffness.**

While these models offer powerful tools for accurately predicting core losses in ferrite materials under various magnetic excitations, they primarily focus on the characteristics of the magnetic excitation itself. They do not account for effects arising from the shape of the ferrite material, i.e., the core geometry, such as e.g. thermally induced mechanical stresses in the ferrite material due to inhomogeneous temperature distributions, as illustrated exemplarily in Fig. 1(b), which is based on the simulation results of an E-core excited by a sinusoidal current i_L and cooled via forced convection. These temperature gradients result in varying thermal expansions of the ferrite material, as can be seen in the simulated displacement shown in Fig. 2(a). Due to the relatively high stiffness of ferrite and its resulting mechanical resistance to deformation, this thermal expansion generates significant thermo-mechanical stress within the material, which can locally easily exceed 10 MPa (cf. Fig. 2(b), potentially increasing the resulting core losses [8]. This paper consequently aims to quantify the influence of such mechanical stresses, which can either be induced thermally or mechanically (by e.g. clamping the core), on the core losses through numerous experimental measurements. Section II introduces the measurement method and the experimental setup which is used to measure the core losses under different mechanical stress conditions. Furthermore, a simple extension of the GSE, named X-GSE, is proposed that captures the general trend of the core losses as a function of mechanical stress, frequency, and flux density, distinguishing between parallel and perpendicular orientations of the flux and stress vectors. In Section III, the dependence of the relative permeability of ferrite on mechanical stress is analyzed, as it affects the flux distribution within the core significantly. In Section IV, the measured results are used to estimate the impact of mechanical stress in an exemplary practical application through FEM simulations. Section V summarizes the key findings of the paper.

II. EXPERIMENTAL SETUP

It has been demonstrated in literature, through both theoretical analyses and experimental measurements, that mechanical tensile and compressive stresses can significantly affect core losses and the relative permeability of ferrite materials [9], [10], [11], [12]. In most cases, experiments involved subjecting a toroidal core to either compressive or tensile stress to investigate the resulting changes in magnetic material parameters. One of the key findings from these studies is that the effect of a given mechanical stress on the material parameters depends on whether the magnetic flux $\vec{B}$ and mechanical stress $\vec{P}$ vectors are aligned or perpendicular to each other. It has also been shown that the relative permeability decreases

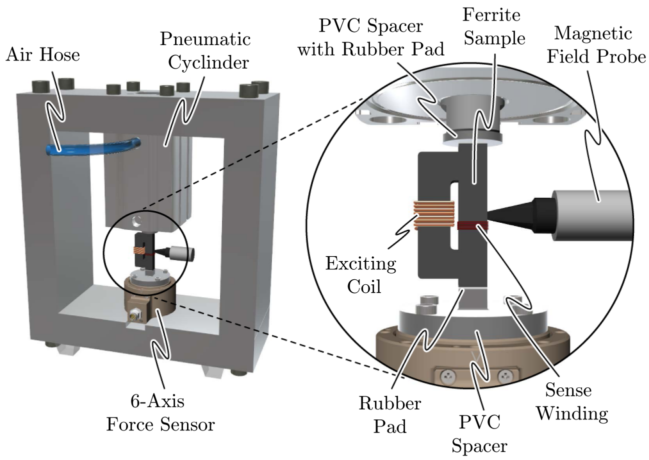

FIGURE 3. Measurement setup for determining the core losses in various ferrite materials under different compressive and tensile stress conditions using the conventional *B-H* curve analysis. The pneumatic cylinder [14] allows for switching from compressive load to tensile load by swapping the supplying air pressure hoses. However, the ferrite sample must be glued to the cylinder's piston for measurements under tensile loads.

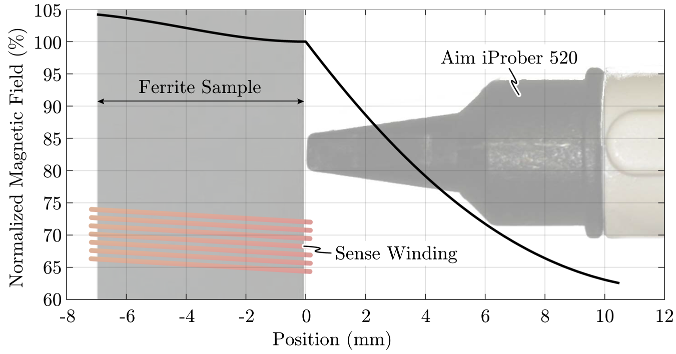

FIGURE 4. Normalized magnetic field strength inside and outside the ferrite sample, along with the probe tip of the H-field sensor (iProber 520), which is shown in correct proportion to the sample. The measurement error of the H-field is within the low single-digit percentage range.

significantly with increasing mechanical stress. Furthermore, in [13], it was mathematically demonstrated that mechanical compression with parallel $\vec{B}$ and $\vec{P}$ vectors has the same effect on core losses as tensile stress with perpendicular $\vec{B}$ and $\vec{P}$ vectors and vice versa. In this paper, we aim to verify these qualitative findings and extend them to enable quantitative predictions of core losses in ferrite materials under mechanical stress.

Since all four combinations of parallel and perpendicular $\vec{B}$ and $\vec{P}$ vectors, under both compressive and tensile stress, can occur in a conventional E-core, it is necessary to measure the core loss dependence of a specific ferrite material under all these conditions to fully characterize it. For this purpose, a setup was developed that subjects I-shaped ferrite samples to these conditions. The advantage of using I-shaped samples over toroidal cores is that it allows for the simple creation of both perfectly perpendicular and parallel $\vec{B}$ and $\vec{P}$ vectors locally. Thus, while toroidal cores allow for generating perfectly perpendicular $\vec{B}$ and $\vec{P}$ vectors only (mechanical stress applied in line with the geometric axis of the toroid), the I-core allows for parallel alignment as well. In the experimental setup at hand, the magnetic flux is applied along the longest dimension of the I-core using an additional U-core with an excitation coil attached to the sample (cf. Fig. 3). A pneumatic cylinder then applies either compression or tension to the I-core, and depending on the sample's orientation, the $\vec{B}$ and $\vec{P}$ vectors are either parallel or perpendicular.

Using a pneumatic cylinder allows for the generation of relatively high mechanical stresses with minimal effort, which can still be controlled precisely. Thus, instead of a more complex hydraulic setup, a simple air compressor or an existing compressed air line, as commonly found as standard equipment in most laboratories, is sufficient to conduct the experiments.

In the proposed experimental setup, the mechanical stress P in the ferrite is calculated using the known cross-sectional area A_I of the ferrite sample and the force F, which is measured by a force sensor, according to

$$P = \frac{F}{A_I}. \tag{2}$$

In order to measure the applied force, a six-axis force and torque sensor (Rokubi - Bota Systems [15]) is employed, as it ensures that uniform stress distributions are maintained in the ferrite sample as long as the torques around the x- and y-axes are zero.

Due to the simplicity of the experimental setup, the desired mechanical and magnetic conditions are confined to specific regions within the ferrite, referred to as local conditions. These conditions imply that the mechanical stress and magnetic field are non-uniformly distributed, i.e. only a limited volume of the material is affected and considered. Accordingly, a measurement method is needed that can capture these localized variations of the core losses and the relative permeability within the ferrite. For this reason, a sensing coil is placed in the center of the I-core, allowing measuring the magnetic flux in the core and, therefore, the flux density B in the ferrite to be determined from the measured induced winding voltage $u_i(t)$ (cf. Fig. 3), according to

$$B(t) = \frac{1}{N \cdot A_I} \int u_i(t)\mathrm{d}t. \tag{3}$$

Directly next to or above the sensing coil, the magnetic field strength H is measured using a magnetic field probe (Aim iProber 520 [16]). Although the magnetic field strength decreases outside the core, the boundary condition that the tangential component of the magnetic field needs to remain constant across material boundaries, allows for a relatively accurate estimation of the H-field within the core based on measurements taken outside, as shown in Fig. 4. Since the primary interest is in the relative change in core losses under increasing mechanical stress, it is not problematic if the H-field is measured with a small margin of error, as this error is consistent across all measurements and does not affect the

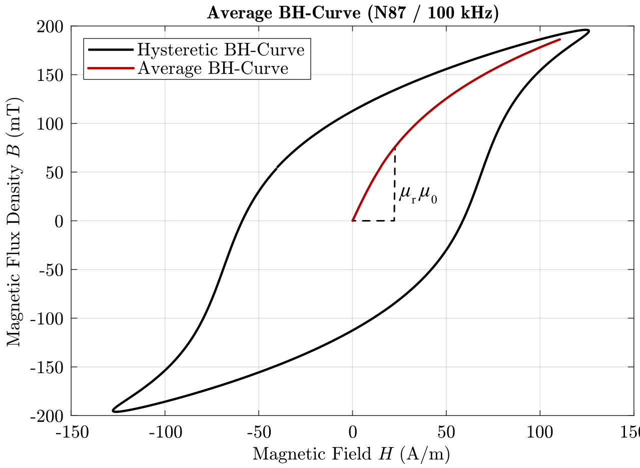

FIGURE 5. Measured hysteretic *B-H* curve (black), where at least five cycles are recorded and subsequently averaged. The average *B-H* curve (red) is calculated by considering the mean value of the left and right boundaries of the hysteretic *B-H* curve.

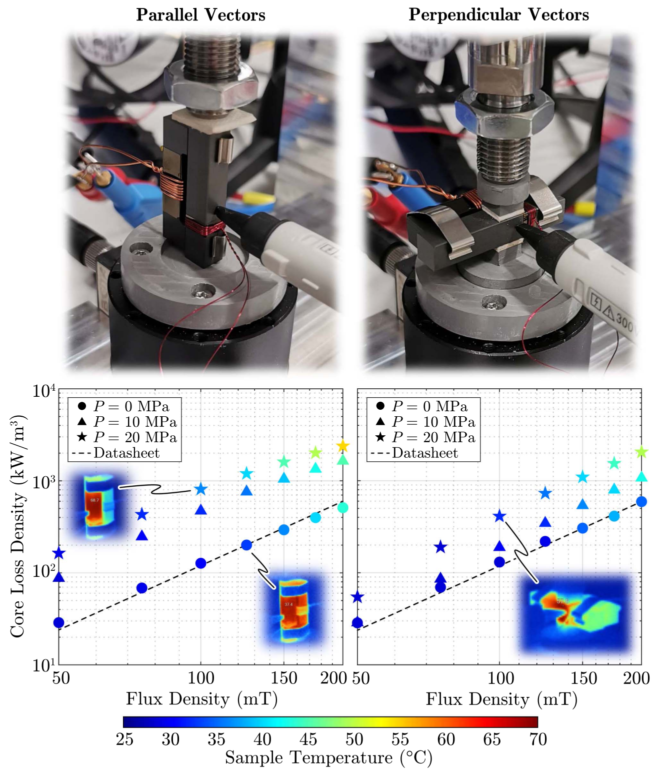

FIGURE 6. Clamped N87 ferrite samples for parallel stress and flux vectors (left) and for perpendicular stress and flux vectors (right), with the corresponding measured core loss densities for different flux densities *B* and compressive mechanical stresses *P* at a frequency of 100 kHz.

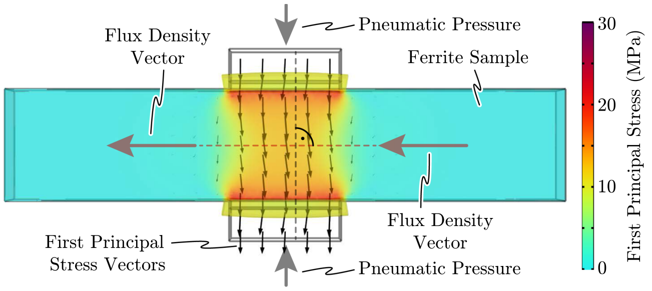

FIGURE 7. Distribution of mechanical stresses in the ferrite sample for perpendicular stress and flux vectors, with the pressure applied from above and below using pneumatic square stamps. Although the mechanical stress is applied only locally, it remains nearly perfectly perpendicular in between the stamps. This can be determined based on the first principal stress vectors, where a negative direction indicates compressive stress, and a positive direction indicates tensile stress.

relative trend of the losses. Finally, the well-known $B-H$ loop can be plotted from the indirectly measured B and H waveforms, and the area enclosed by the loop represents the energy E_C lost per cycle (cf. Fig. 5). By multiplying this energy E_C by the switching frequency f_{sw}, the local core loss density p_C in the ferrite sample can be determined. This measurement method allows for rapid evaluation of core loss densities under a wide range of operating conditions. As an example, Fig. 6 shows the measured core loss densities in N87 at a switching frequency of 100 kHz and different compressive stress values (0 MPa, 10 MPa, 20 MPa). On the left, the setup and results for parallel $\vec{B}$ and $\vec{P}$ vectors are shown, while on the right, the same is presented for perpendicular $\vec{B}$ and $\vec{P}$ vectors. Two main conclusions can be drawn from these results. First, the measurement method demonstrates good accuracy, as the measured core loss densities without mechanical stress match well with the datasheet values. Second, as expected, the direction of the mechanical stress relative to the magnetic flux has a significant impact on the resulting core losses. Furthermore, thermal images taken without cooling of the I-core sample clearly demonstrate that the core losses increase significantly under stress. This is evident as the I-core heats up much more than the U-core, even though both cores are subjected to the same magnetic flux densities. For this reason, it is crucial to cool the sample as effectively as possible using forced convection during measurements. Otherwise, the temperature dependence of the core losses could significantly distort the measurement results, as evident from the data points in Fig. 6, where a clear trend shows that core losses decrease with increasing temperature.

It should be noted that in the setup for perpendicular $\vec{B}$ and $\vec{P}$ vectors, the mechanical stress is only generated locally in a relatively small volume (cf. Fig. 7). However, in between the two pressure plates applying the desired mechanical stress, the stress vectors $\vec{P}$ align as intended, perpendicular to the magnetic flux density $\vec{B}$. Thus, as long as the H-field is measured in the center between the pressure plates, the core losses can be measured under the desired mechanical and magnetic conditions. Furthermore, as previously mentioned, a certain measurement error due to the setup has no impact on the relative dependence of the losses on the mechanically applied stress, which is why this approach is a good compromise between measurement accuracy and simplicity of the setup.

To fully characterize the behavior of a ferrite material under mechanical stresses, it would theoretically be necessary to

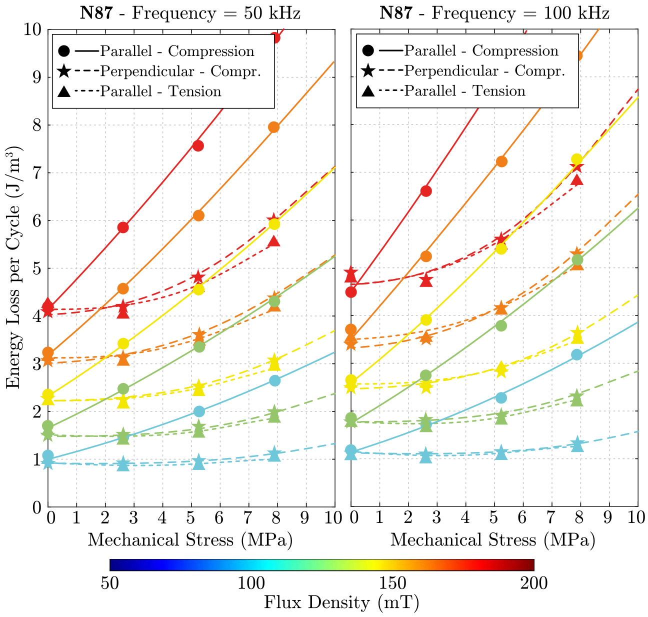

FIGURE 8. Energy losses per cycle in N87 at 50 kHz and 100 kHz under different tensile and compressive stress conditions for flux and force vectors that are either parallel or perpendicular to each other.

measure the core losses under both compressive and tensile stresses for different vector orientations. However, measuring under tensile stress is not straightforward, as securing the I-core mechanically to the pneumatic cylinder is quite challenging due to the small contact area. However, in [13], it is shown that the ferrite material behaves similarly under tensile stress with parallel $\vec{B}$ and $\vec{P}$ vectors as it does under compressive stress with perpendicular $\vec{B}$ and $\vec{P}$ vectors (and vice versa). Experimentally, only the analogy for the case of tensile stress with parallel $\vec{B}$ and $\vec{P}$ vectors and compressive stress with perpendicular $\vec{B}$ and $\vec{P}$ vectors could be verified (cf. Fig. 8), as generating well-defined tensile stress with perpendicular $\vec{B}$ and $\vec{P}$ vectors is particularly challenging in the measurement setup of Fig. 3. Nevertheless, based on physical principles, it is reasonable to assume that the analogy also holds for the reverse case. Consequently, this allows for a complete characterization of the ferrite material using only two measurement series under compressive conditions (with parallel and perpendicular $\vec{B}$ and $\vec{P}$ vectors).

First, an I-core made of N87 ferrite material was subjected to excitation with sinusoidal magnetic flux at frequencies of 50 kHz, 100 kHz, and 200 kHz, where the $\vec{B}$ and $\vec{P}$ vectors were aligned in parallel. The amplitudes of the flux densities in the I-core, as well as the mechanical stress applied to the core, were varied across a wide range. The measured data points are shown in Fig. 9 as blue dots, clearly indicating that the core losses increase significantly with rising stress values P. During the measurements, care was taken to ensure that the sample did not experience significant heating (a maximum temperature rise of approximately 25 °C), so that the temperature dependence of the core losses would not have too much influence on the results. This is achieved through a combination of forced convection cooling and a cool-down sequence of the sample between individual measurements. This approach leverages the thermal capacity of the ferrite, which delays the material's temperature increase, allowing relatively high loss densities (up to 5 MWm^{-3}) to be measured even at lower temperatures. When examining the relationship between the core losses and the applied mechanical stress more closely, an almost linear dependency is observed within the tested compressive stress range. This makes it possible to capture the stress dependence of the losses with a simple extension of the Generalized Steinmetz Equation (GSE), according to

$$p_C = C \cdot f^{\alpha} \cdot B^{\beta} \cdot (1 + \gamma_{=} \cdot P), \tag{4}$$

which is referred to as eXtended GSE (X-GSE) in the following. Thus, by introducing a single additional Steinmetz parameter $\gamma_{=}$, along with the corresponding equation, the core losses under compressive stress, where the stress is aligned with the direction of the magnetic flux, can be easily estimated. Despite the simplicity of the X-GSE, this approach proves surprisingly effective for making initial estimates of the core losses, as demonstrated by the relative error of the individual data points in Fig. 9, which indicate the relative difference between the measured data points and the semi-transparent surfaces calculated based on (4) with $C = 1.37$ [$\mathrm{Wm^{-3}Hz^{-\alpha}T^{-\beta}}$], $\alpha = 1.49$, $\beta = 2.36$ and $\gamma_{=} = 2.21\mathrm{e}-7$ [$\mathrm{Pa^{-1}}$]. The largest deviations occur at low flux densities and mechanical stresses, and consequently at low loss densities as well.

The same measurement series was subsequently conducted for perpendicular $\vec{B}$ and $\vec{P}$ vectors under otherwise identical conditions, revealing a different dependence of the core losses on the applied mechanical compressive stress. As can be seen from the data points in Fig. 10, there exists a minimum stress value P_0 for N87 ferrite, below which the additional stress has no significant impact on the core losses (approximately 5 MPa). Only beyond this minimum stress value do the core losses start to increase, again approximately linearly within the tested compressive stress range. This behavior can be represented through a two-part extension of the GSE, according to

$$p_C = \begin{cases} C \cdot f^{\alpha} \cdot B^{\beta} & \text{if } P < P_0, \\ C \cdot f^{\alpha} \cdot B^{\beta} \cdot (1 + \gamma_{+} \cdot (P - P_0)) & \text{if } P \geq P_0. \end{cases} \tag{5}$$

where γ_{+} denotes a second extended Steinmetz parameter. Although this very simple fitting function, with its minimal number of parameters, does not fully capture the complex dependencies of the core losses on the various physical parameters, it still provides a reasonably accurate estimate of the core losses, especially for higher flux densities. This can be concluded from the relative errors between the measured values and the values calculated from (5) for the individual data points, as shown in Fig. 10.

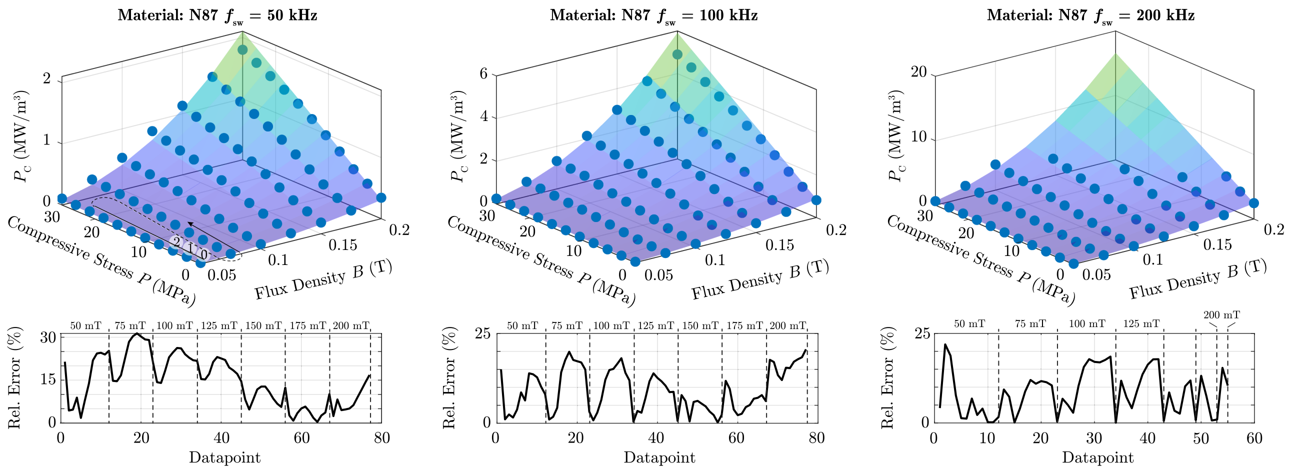

FIGURE 9. Measured core loss densities (blue dots) and calculated values (shaded areas) using the X-GSE function (4) for parallel mechanical stress and magnetic flux vectors, under varying mechanical compressive stresses P, flux densities B, and switching frequencies f_{sw} for N87 ferrite material. Additionally, the relative errors are shown for all data points.

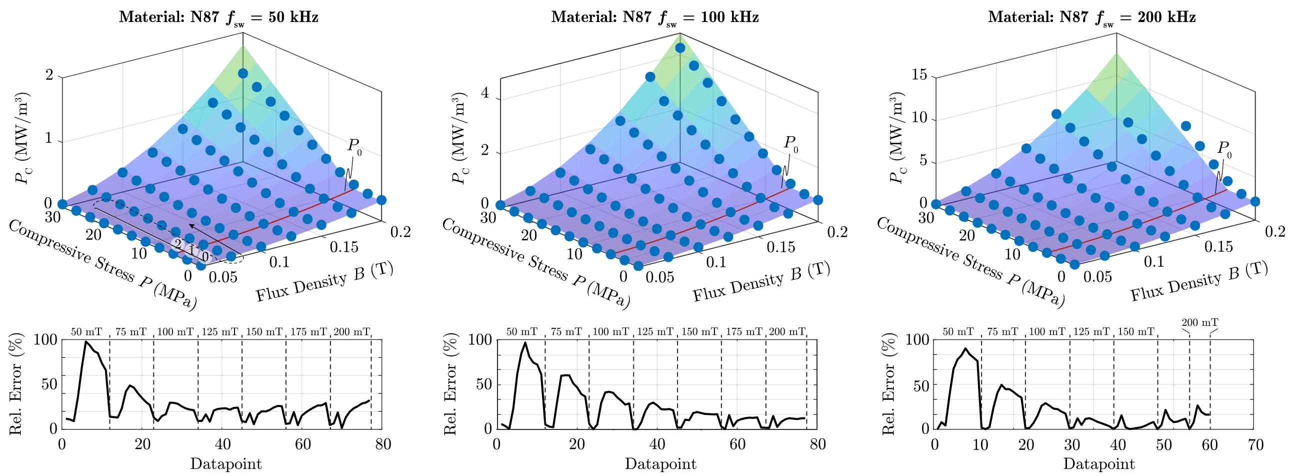

FIGURE 10. Measured core loss densities (blue dots) and calculated values (shaded areas) using the X-GSE function (5) for perpendicular mechanical stress and magnetic flux vectors, under varying compressive stresses P, flux densities B, and switching frequencies f_{sw} for N87 ferrite material. Additionally, the relative errors are shown for all data points.

Given the simplicity of the proposed X-GSE and the small number of additional fitting parameters, it is theoretically possible to fully characterize the stress-dependent behavior of a known ferrite material (with known C, α, and β parameters) using just two measurement sets: one with parallel $\vec{B}$ and $\vec{P}$ vectors and one with perpendicular vectors, each at a single frequency and flux density for varying stress values.

However, in practice, it is advisable to determine the extended Steinmetz parameters — $\gamma_{=}$, γ_{+}, and P_0 — using a larger number of measurement sets to achieve high predictive accuracy over a broader range. This approach was applied not only to the widely used N87 ferrite material but also to three additional materials (N49, 3C95, and 3C97), with the corresponding X-GSE parameters summarized in Table 1. The parameters were determined using a least-squares error (LSQ) fit, where in a first step, the three parameters α, β, and C were calculated based on the measurement data without any external mechanical stress ($P = 0\,\mathrm{MPa}$). Subsequently, the parameters $\gamma_{=}$, γ_{+}, and P_0 were determined using a second LSQ fit, but this time applied to all data points. As an alternative approach, one could impose a constraint by using identical C-values and then fitting α and β. This would yield only marginally larger relative errors for the fitting functions, but physically more reasonable identical C values. As can be seen based on these parameters, there are significant differences between the materials in how they respond to mechanical stress. However, all the measured materials share a common characteristic: the core losses increase significantly as mechanical stress increases, which could lead to a substantial increase in core losses in a real application. However, not only do core losses change with increasing mechanical stress, but also the permeability of the material

TABLE 1. Extended Steinmetz Parameters for the Proposed X-GSE

Material	Direction	C [$\mathrm{Wm^{-3}Hz^{-\alpha}T^{-\beta}}$]	α	β	$\gamma_{=}$ [$\mathrm{Pa^{-1}}$]	γ_{+} [$\mathrm{Pa^{-1}}$]	P_0 [Pa]
N87	Parallel	1.37	1.49	2.36	2.21e-7		
	Perpendicular	3.07	1.41	2.31		2.34e-7	5.41e6
N49	Parallel	10	1.44	2.98	3.17e-7		
	Perpendicular	10	1.43	2.99		2.33e-7	3.89e6
3C95	Parallel	1.09	1.50	2.58	2.96e-7		
	Perpendicular	1.08	1.50	2.61		3.43e-7	2.27e6
3C97	Parallel	0.84	1.55	2.81	4.79e-7		
	Perpendicular	1.98	1.46	2.78		4.73e-7	6.1e6

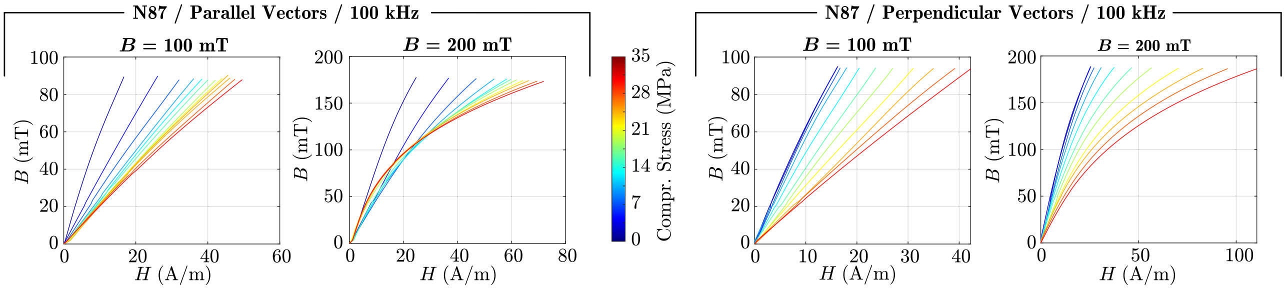

FIGURE 11. Average B-H curves for parallel and perpendicular mechanical stress and magnetic flux vectors, under varying compressive stresses, flux densities B, and switching frequencies f_{sw} for N87 ferrite material.

is affected. This will be examined in more detail in the next section.

III. STRESS DEPENDENCE OF THE RELATIVE PERMEABILITY

The same B-H curves, which were measured for the core loss calculations, can also be used to infer the relative permeability of the material under mechanical stress conditions. For each measurement, an average B-H curve can be calculated as shown in Fig. 5. The average B-H curves for different compressive stress conditions and $\vec{B}$ and $\vec{P}$ vector orientations can then be compared (see Fig. 11). The results show a clear decrease in relative permeability, indicated by the reduction in the slope of the average B-H curves, with increasing stress levels. Notably, the behavior differs significantly between the parallel and perpendicular cases.

In the parallel configuration, increasing mechanical stress leads to a continuous reduction in μ_r, as seen in the measured average B-H curves in Fig. 11. This behavior is expected, as compressive stress potentially inhibits the movement of magnetic domains, reducing the material's ability to magnetize, and consequently decreasing its permeability. Fig. 12 shows the maximum and minimum relative permeabilities at different stress levels, confirming this trend for different magnetic flux densities. The maximum and minimum relative permeabilities correspond to the steepest and flattest slopes of the average B-H curves of Fig. 11, respectively.

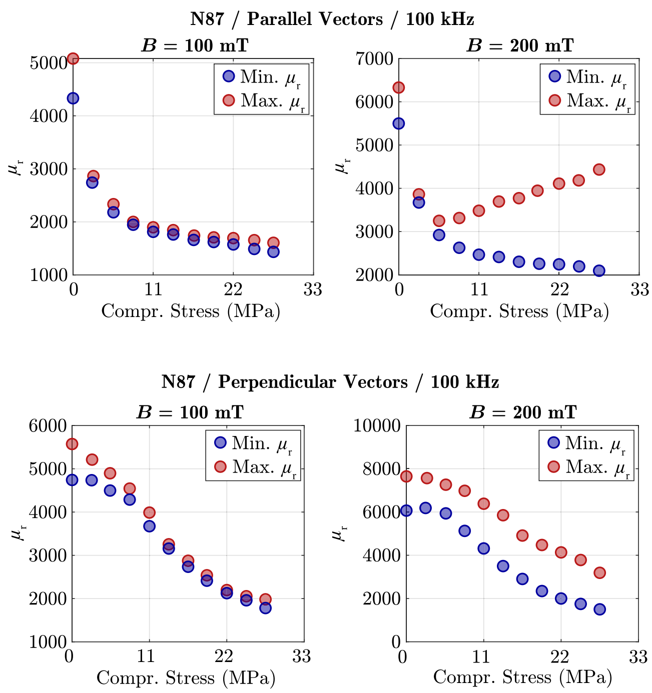

FIGURE 12. Minimum and maximum relative permeabilities for parallel and perpendicular mechanical stress and magnetic flux vectors, under varying compressive stresses, for different flux densities B, and a switching frequency f_{sw} of 100 kHz for N87 ferrite material.

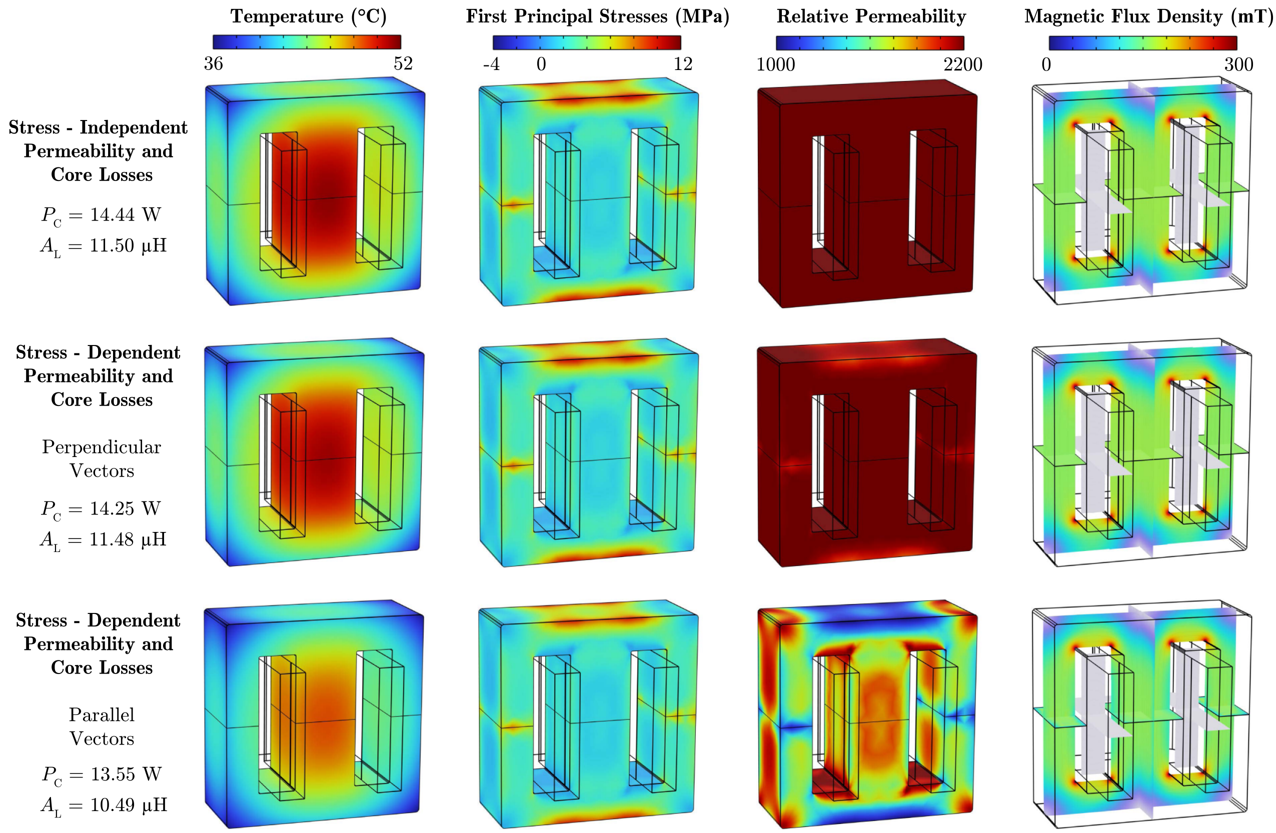

FIGURE 13. Temperature distributions in an E65/32/27 core simulated in COMSOL, along with the resulting first principal stresses, the relative permeability of the core material, and the magnetic flux density distribution. The simulation was conducted three times, with the magnetic flux in the core being excited in each case by a uniformly distributed current through the winding windows, represented by black-framed cuboids. In the first case, a classical approach with stress-independent core losses and permeabilities was used. In the second case, stress-dependent core losses and permeabilities were considered, assuming perpendicular stress and flux vectors. In the third case, the same stress-dependent losses and permeabilities were applied, but with parallel stress and flux vectors. In all simulations, the inductors are potted in a cube-shaped silicone block with a constant surface temperature of 25 °C, and the following core material parameters were consistently applied: $\nu_{N87} = 0.3$, $\sigma_{N87} = 4.5\,\mathrm{W/m\,K^{-1}}$, $E_{N87} = 120\,\mathrm{GPa}$, $\alpha_{N87} = 11 \times 10^{-6}\,\mathrm{K^{-1}}$.

For perpendicular vectors, the reduction in μ_r is less pronounced, with a noticeable plateau at lower stress levels. This suggests that the material better tolerates mechanical stress when the flux and stress vectors are perpendicular, maintaining a higher permeability in this configuration. The decreased sensitivity to mechanical stress in the perpendicular case can be attributed to the anisotropic response of ferrite under different stress orientations.

Overall, the changes in μ_r significantly affect the distribution of the magnetic flux density within the core, as areas with reduced permeability divert the magnetic flux, leading to non-uniform flux distributions. This can be visualized through FEM simulations that incorporate the measured core loss and permeability responses at different stress levels, as discussed in more detail in the following section.

IV. INFLUENCE OF TEMPERATURE-INDUCED MECHANICAL STRESSES ON THE FLUX DENSITY DISTRIBUTION

To investigate the general impact of thermally induced stresses on the core losses, coupled FEM simulations can be employed. These simulations iteratively solve (i) electromagnetic (core losses), (ii) thermal (temperature distribution within the core), and (iii) mechanical (mechanical stresses) fields until convergence is achieved. Due to the significantly varying local conditions in conventional core geometries with respect to the directions of flux and stress vectors, accurately simulating the effective core losses based on the measured data is challenging. However, best-case and worst-case core losses can be estimated through two separate simulations.

In the best-case simulation, it is assumed that the flux and stress vectors are parallel in regions with tensile stresses and perpendicular in regions with compressive stresses, as these configurations minimize the mechanical stress's influence on the local core losses and the permeability. The core losses are therefore modeled using (5), and the permeability is set relative to the μ_r-curve shown in Fig. 12 for perpendicular vectors and flux density of 100 mT, which is the average flux density in core of the simulation.

In the worst-case simulation, the opposite is assumed: the flux and stress vectors are perpendicular in regions with tensile stresses and parallel in regions with compressive stresses. In this scenario, the core losses are modeled using (4), and the permeability is again calculated relative to the μ_r-curve shown in Fig. 12 for a flux density of 100 mT, but this time the one for parallel vectors.

Finally, a reference simulation is performed in which no stress dependence of the material parameters is considered. Here, a homogeneous permeability is assumed and the core losses are calculated based on the GSE. The results of the three simulations are shown in Fig. 13, where several notable effects can be observed. One key observation is that considering the stress dependence leads to a slight decrease in simulated losses. This is because mechanical stresses reduce the local permeability in the ferrite, which displaces the magnetic flux from these regions, thereby lowering the local magnetic flux density and, consequently, the local core loss density. To simplify somewhat, the stress-dependent permeability causes the magnetic flux to be naturally redistributed to regions where lower core losses occur, while avoiding areas where high core losses would otherwise occur.

However, the stress dependence of the permeability also causes a reduction in the average relative permeability of the core material, leading to a decrease in the inductance or the A_L value of the core (up to 9% in the worst-case scenario). These results are valid only for the simulation setup considered, where the E-core and the winding are potted in a cube-shaped thermally conductive silicone block that can expand freely in all directions, thus not exerting external mechanical stresses on the core. The surfaces of the silicone block are set to a constant temperature of 25 °C, ensuring a controlled thermal environment during the simulation. However, if additional external stresses are applied to a core, significantly higher mechanical stresses can arise, potentially causing much higher core losses than those calculated by neglecting the stress dependence of core losses. This can escalate to a point where thermal cracks develop in the ferrite, leading to permanent damage of the component. Therefore, it is crucial to account for the stress dependence of the core losses in ferrite, especially when designing magnetic components that will be potted in incompressible materials as e.g. epoxy resin or silicone in an enclosed housing.

V. CONCLUSION

This paper extends the Generalized Steinmetz Equation (GSE) into a new X-GSE to include the effects of mechanical stress on the core losses in ferrite materials. Experimental results confirm that the relative permeability and core losses are strongly influenced by mechanical stress, with significant differences depending on the orientation of the magnetic flux density and stress vectors. Parallel vectors lead to a more pronounced reduction in permeability and an increase in core losses under mechanical compressive stress (pressure), while perpendicular vectors exhibit a more complex, stress-dependent response.

FEM simulations further demonstrate that thermally induced mechanical stresses in an E-core lead to a redistribution of magnetic flux, which can either increase or decrease core losses depending on the stress levels and material properties. In cases of moderate mechanical stress, core losses are reduced due to a more homogeneous flux distribution. However, under higher mechanical stress conditions, particularly when thermal expansion is constrained, core losses can increase significantly.

These findings highlight the need to account for mechanical stress effects in core loss calculations, especially in applications where steep temperature gradients or external mechanical constraints are present. By incorporating a stress-dependent core loss component into the Steinmetz equation, this work provides a more comprehensive model for predicting core losses, paving the way for more accurate designs and optimizations of magnetic components in power electronic systems.

While the results presented in this paper provide a solid foundation for extending the GSE to account for mechanical stress effects on the core losses, they are not exhaustive. The physical mechanisms underlying these observations remain complex and require further measurements and investigations to be fully understood. Thus, it could theoretically be possible to attempt coupling the X-GSE with the temperature model from [6], as both models rely on multiplying the GSE by an additional factor. This approach would allow applying both factors to the GSE simultaneously, thereby accounting for both temperature dependence and the influence of mechanical stresses. However, our goal in this initial study was to provide an empirical foundation for engineers to incorporate stress-dependence in core loss calculations, enabling more accurate design considerations.

REFERENCES

[1] C. P. Steinmetz, "On the law of hysteresis," *Trans. Amer. Inst. Elect. Engineers*, vol. IX, no. 1, pp. 1–64, 1892.

[2] E. Snelling, *Soft Ferrites, Properties and Applications*. London, U.K.: Butter Worth and Co Ltd., 1988.

[3] J. Reinert, A. Brockmeyer, and R. De Doncker, "Calculation of losses in ferro- and ferrimagnetic materials based on the modified Steinmetz equation," *IEEE Trans. Ind. Appl.*, vol. 37, no. 4, pp. 1055–1061, Jul./Aug. 2001.

[4] K. Venkatachalam, C. Sullivan, T. Abdallah, and H. Tacca, "Accurate prediction of ferrite core loss with nonsinusoidal waveforms using only Steinmetz parameters," in *Proc. IEEE Workshop Comput. Power Electron.*, 2002, pp. 36–41.

[5] J. Muhlethaler, J. Biela, J. W. Kolar, and A. Ecklebe, "Core losses under the DC bias condition based on Steinmetz parameters," *IEEE Trans. Power Electron.*, vol. 27, no. 2, pp. 953–963, Feb. 2012.

[6] J. Y. Alsawalhi and S. D. Sudhoff, "Saturable thermally-representative Steinmetz-based loss models," *IEEE Trans. Magn.*, vol. 49, no. 11, pp. 5438–5445, Nov. 2013.

[7] J. Muhlethaler, J. Biela, J. W. Kolar, and A. Ecklebe, "Improved core-loss calculation for magnetic components employed in power electronic systems," *IEEE Trans. Power Electron.*, vol. 27, no. 2, pp. 964–973, Feb. 2012.

[8] A. K. Bailey, J. Sun, S. Kim, W. Wijaya, T. Allen, and G. A. Covic, "Effects of compressive stress on ferrites in inductive power transfer," in *Proc. 2025 IEEE Wireless Power Technol. Conf. Expo.*, 2025.

[9] E. Snelling, "The effects of stress on some properties of MnZn ferrite," *IEEE Trans. Magn.*, vol. TMAG-10, no. 3, pp. 616–618, Sep. 1974.

[10] Z. Li et al., "Effect of compressive stress on power loss of Mn–Zn ferrite for high-frequency applications," *Ceramics Int.*, vol. 48, pp. 17723–17728, 2022.

[11] V. Tsakaloudi, D. Holz, and V. Zaspalis, "The effect of externally applied uniaxial compressive stress on the magnetic properties of power MnZn-ferrites," *J. Mater. Sci.*, vol. 48, pp. 3825–3833, 2013.

[12] T. Thomas et al., "Ferrite embedding for power SiPs - A packaging view," in *Proc. 10th Int. Conf. Integr. Power Electron. Syst.*, 2018, pp. 1–6.

[13] M. Baumann, S. Sotier, and J. Weidinger, "A model of initial permeability of soft ferrite in dependence of biaxial stress," *J. Jpn. Soc. Powder Powder Metall.*, vol. 61, pp. S70–S74, 2014.

[14] Festo, "ADN-S-50-50-I-P-A - compact double-acting pneumatic cylinder," 2024. [Online]. Available: https://www.festo.com/ch/de/c/produkte/antriebe-aktuatoren/

[15] Bota-Systems, "Rokubi - compact and robust 6 axis force torque sensor," 2024. [Online]. Available: https://www.botasys.com/force-torque-sensors/rokubi

[16] AimTTi, "I-Prober 520 - high accuracy general purpose h-field probe," 2024. [Online]. Available: https://www.aimtti.com/product-category/current-probes/aim-i-prober-520